ARMY RESEARCH LABORATORY

Time Reversal Methods for Structural Health Monitoring of Metallic Structures Using Guided Waves

by Robert F. Anastasi

ARL-TR-5716 **September 2011**

NOTICES

Disclaimers

The findings in this report are not to be construed as an official Department of the Army position unless so designated by other authorized documents.

Citation of manufacturer‘s or trade names does not constitute an official endorsement or approval of the use thereof.

Destroy this report when it is no longer needed. Do not return it to the originator.

Army Research Laboratory
NASA Langley Research Center, MS231, Hampton, VA 23681

ARL-TR-5716 **September 2011**

Time Reversal Methods for Structural Health Monitoring of Metallic Structures Using Guided Waves

Robert F. Anastasi
Vehicle Technology Directorate, ARL

REPORT DOCUMENTATION PAGE

Form Approved
OMB No. 0704-0188

1. REPORT DATE *(DD-MM-YYYY)*	2. REPORT TYPE	3. DATES COVERED (From - To)
September 2011	Final	10/25/2010–06/21/2011

4. TITLE AND SUBTITLE
Time Reversal Methods for Structural Health Monitoring of Metallic Structures Using Guided Waves

5a. CONTRACT NUMBER

5b. GRANT NUMBER

5c. PROGRAM ELEMENT NUMBER

6. AUTHOR(S)
Robert F. Anastasi

5d. PROJECT NUMBER

5e. TASK NUMBER

5f. WORK UNIT NUMBER

7. PERFORMING ORGANIZATION NAME(S) AND ADDRESS(ES)
U.S. Army Research Laboratory,
Vehicle Technology Directorate, Mechanics Division, RDRL-VTM,
Nondestructive Evaluation Sciences Branch,
NASA Langley Research Center, MS231, Hampton, VA 23681

8. PERFORMING ORGANIZATION REPORT NUMBER
ARL-TR-5716

9. SPONSORING/MONITORING AGENCY NAME(S) AND ADDRESS(ES)

10. SPONSOR/MONITOR'S ACRONYM(S)

11. SPONSOR/MONITOR'S REPORT NUMBER(S)

12. DISTRIBUTION/AVAILABILITY STATEMENT
Approved for public release; distribution unlimited.

13. SUPPLEMENTARY NOTES

14. ABSTRACT
Time reversal methods for ultrasonic guided waves are being investigated for detecting damage in metallic plate structures. According to this method the input signal to a system can be reconstructed if a response signal obtained from another point is emitted back to the original point after being reversed in time. Damage diagnosis lies in the premise that the time reversibility breaks down when a certain type of defect such as nonlinear damage exists along the wave propagation path. The defect can then be sensed by correlating the reconstructed signal with the original signal. The difficulty of direct application lies in the fact that ultrasonic guided waves disperse while propagating thus will not totally reconstruct the original signal. Overcoming this difficulty is examined in a finite difference model with narrow and broadband excitation of guided waves in a metallic plate with damage simulated as a shallow notch. Results show that narrow band excitation is somewhat more sensitivity then broadband excitation to notch depth.

15. SUBJECT TERMS
Lamb waves, guided waves, time reversal, damage, notch

16. SECURITY CLASSIFICATION OF:			17. LIMITATION OF ABSTRACT	18. NUMBER OF PAGES	19a. NAME OF RESPONSIBLE PERSON
a. REPORT	b. ABSTRACT	c. THIS PAGE	UU	31	Amy Pancio
Unclassified	Unclassified	Unclassified			19b. TELEPHONE NUMBER (*Include area code*) (410) 278-8697

Contents

List of Figures

INTENTIONALLY LEFT BLANK.

1. Introduction

Mechanical engineering structures such as aerospace and civil infrastructures are being built with new material or materials that require greater integrity and reliability. It is often necessary to ensure and monitor the integrity of these material structures for continued reliable performance. Guided wave based nondestructive evaluation methods is one method that can be used to monitor and detect damage in plate like structural materials by examination of Lamb wave time-domain signals (*1, 2*) where the existence of damage is inferred by correlating a currently measured signal with a baseline signal. For large structure and numerous sensors, a file of baseline signals makes using this method a complex task. A potential method to eliminating the use of baseline signals would be to use time-reversal methods (TRM). These methods were introduced and used in 2D and 3D to focus and steer acoustic beams in inhomogeneous media (*3–5*) for application to lithotripsy. Chakroun et al. (*6, 7*) demonstrated the use of TRM in detecting small defect in solid material and the ability to compensate for the distortions introduced by liquid-solid interfaces of different geometries. In further work, Roux et al. (*8*) demonstrated how TRM could be used to overcome multipath distortion in acoustic waves and concluded that both time and spatial compression of the time reversed wave field might be useful for underwater acoustics and medical imaging. In nondestructive applications Ing and Fink (*9*) showed how the use of a TRM could automatically compensate for the dispersion nature of Lamb waves, but focusing was limited due to Lamb wave dispersion and Prada et al. (*10*) demonstrates TRM adaptive methods that improve flaw detection through inhomogeneous and scattering media. More TRM and guided wave applications were investigated by Wang et al. (*11, 12*) where they demonstrated that both spatial and temporal focusing can be achieved with dispersive Lamb waves. Xu and Giurgiutiu (*13*) also looked at Lamb waves and TRM and developed a theoretical model for the analysis of Lamb wave time reversal using piezoelectric wafer active sensors and showed that Lamb waves are fully time reversible only when single mode Lamb waves are excited.

In this report, the application of TRM to Lamb wave propagation continues to be investigated for detecting a notch (simulated damage) in a metallic plate. Sensitivity to notch depth is examined with broadband and narrow band excitation in a finite difference model and damage is characterized by comparing source and reconstructed signals.

2. Lamb Waves

Guided waves or Lamb waves are formed by the interference of multiple reflections and mode conversions of longitudinal and shear waves at the free surfaces of a plate. These waves are typically generated and detected using conventional piezoelectric transducers, oriented either flat

or at an angle in respect to the surface and are used to detect defects and measure elastic properties of thin isotropic materials and laminated composite plates. Two types of waves propagate a symmetric wave and antisymmetric wave and each of these wave types propagate with multiple modes. The symmetrical modes move in a symmetrical fashion about the median plane of the plate and are sometimes called extensional mode because the wave is "stretching and compressing" the plate in the wave motion direction. The antisymmetric mode is often called the "flexural mode" because a large portion of the motion moves in a normal direction to the plate, and a little motion occurs in the direction parallel to the plate. In this mode, the body of the plate bends as the two surfaces move in the same direction.

By solving a boundary value problem for a free plate or by considering the reflection of waves at plate boundaries the Rayleigh-Lamb frequency equations (dispersion equations) can be found (*14–17*). For a uniform traction free isotropic plate the equation for symmetric modes is

$$\frac{tan(qh)}{tan(ph)} = -\frac{4k^2pq}{\left(q^2-k^2\right)^2} \tag{1}$$

and for antisymmetric modes

$$\frac{tan(qh)}{tan(ph)} = -\frac{\left(q^2-k^2\right)^2}{4k^2pq} \tag{2}$$

where

$$p^2 = \frac{\omega^2}{c_L^2} - k^2 \text{ and } q^2 = \frac{\omega^2}{c_T^2} - k^2 \text{ and } k = \omega / c_P \tag{3}$$

and h, k, c_L, c_T, c_P, ω are the half-plate thickness, wave number, velocities of longitudinal and transverse modes, phase velocity, and wave circular frequency, respectively.

The phase velocity is found numerically by solving for the real roots of the dispersion equation as a function of material properties, frequency, and material thickness. Group velocity dispersion curves are found from the phase velocity (*17*).

Phase and group velocity dispersion curves for a 2.0-mm thick aluminum plate are shown in figure 1, where longitudinal velocity (c_L), transverse velocity (c_T), and density (ρ) of the plate are equal to 6,420 m/s, 3,040 m/s, and 2,700 kg/m^3, respectively. These curves were generated and plotted using a commercial software package (*18*). At low frequencies the wave velocity of the first symmetric mode (S_0) is nearly non-dispersive while the wave velocity of the first antisymmetric mode (A_0) is highly dispersive and at higher frequencies phase velocity of both

zero order modes approach the Rayleigh wave velocity, c_R, which has a value of approximately 2.9 km/s (*14*) for aluminum with a Poisson's ratio $\nu = 0.33$.

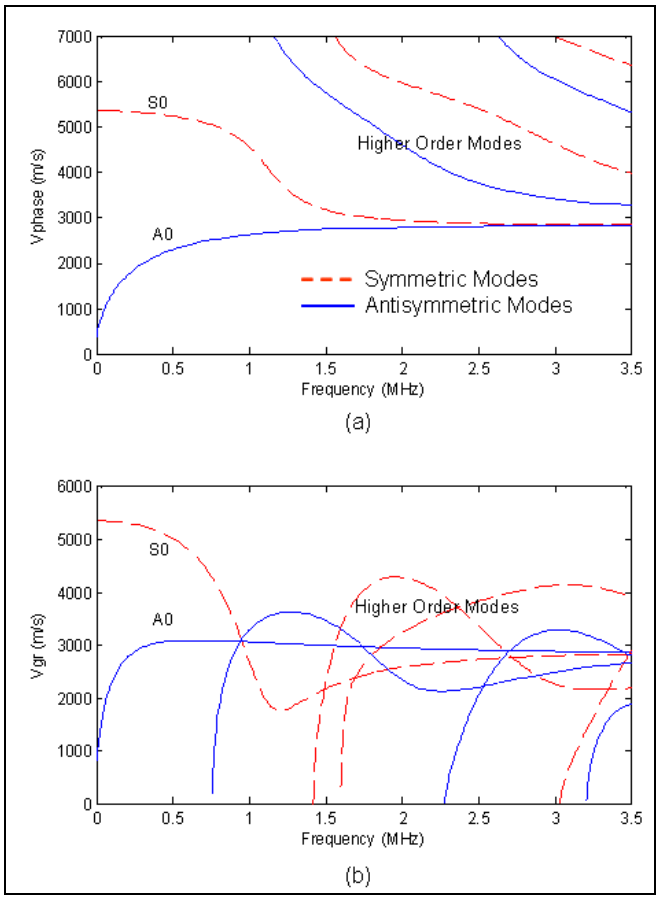

Figure 1. Dispersion curves for 2.0-mm thick aluminum plate (a) phase velocity and (b) group velocity vs. frequency. Where S_0 and A_0 are first order symmetric and antisymmetric Modes respectively.

3. Time Reversal Method

Acoustic time reversal is based in the time-invariant and spatial reciprocity of an acoustic wave propagating in a medium. The time invariance means that the input to a system *now* or *T* seconds from *now* will be identical except for a time delay of *T* seconds. So the system output does not depend on the time the input is applied. The spatial reciprocity means that the position of a source and receiver can be interchanged without altering the resulting field. Thus the reception of a signal at point-A from a source at point-B is the same as the reception of a signal at B from a source at A. This reciprocity breaks down if the signal propagating from point-A to B is disrupted or changed (encounters damage).

The time reversal procedure consists of: (1) applying a source excitation at point-A, (2) recording the response at point-B, (3) time reversing the response at B and emitting it, and (4) record the time reversed wave (the reconstructed wave) at point-A and compare it to the original signal.

In this time reversal procedure wave propagation from point-A to point-B and can be modeled as a convolution operation. If at point-A we have a signal $s_A(t)$ and system transfer function h(t) then the received signal at point-B is given as

$$s_B(t)=s_A(t)*h(t) \tag{4}$$

where * is the convolution operator and transducer transmit and receive transfer function are neglected for simplification. In the frequency domain this becomes

$$S_B(\omega)=S_A(\omega)\cdot H(\omega) \tag{5}$$

where ω is the angular frequency, $S_A(\omega)$, $S_B(\omega)$, and $H(\omega)$ are the Fourier Transforms of the signals $s_A(t)$ and $s_B(t)$, and the system transfer function h(t), respectively.

In the second part of the process, the signal at point-B is reversed in time $s_B(-t)$ which is equivalent to the negative of the angular frequency. The time reversed signal at point-B is given by

$$S_B(\omega)=S_A(-\omega)\cdot H(-\omega)\ . \tag{6}$$

This time reversed signal is then transmitted at point-B and received at point-A. The new signal at point-A is the reconstructed wave and is given by

$$\begin{aligned} S_R(\omega)&=S_B(\omega)\cdot H(\omega) \\ &=S_A(-\omega)\cdot H(-\omega)\cdot H(\omega)\ . \end{aligned} \tag{7}$$

Assuming real and even signals and the transfer function is independent of propagation direction $f(\alpha)=f(-\alpha)$ then the equation 7 can be rewritten as

$$\begin{aligned} S_R(\omega)&=S_A(\omega)\cdot H(\omega)\cdot H(\omega) \\ &=S_A(\omega)\cdot H^2(\omega)\qquad\ . \end{aligned} \tag{8}$$

Equation 8 shows that the reconstructed signal has the same profile as the source signal

4. Damage Index

Damage detection using the TRM is accomplished by comparing the source excitation signal with the reconstructed signal. The deviation between these signals is typically quantified using a damage index (DI). Several damage metrics have been used to compare signals and assess the presence of damage. The most popular choices for a DI are root mean square error (RMSE) and power spectral density (PSD). Also considered are signal maximum value (MAX) and maximum value of the signals amplitude spectrum (SPMX).

4.1 Root Mean Squared Error (RMSE)

RMSE is a measure of the differences between two signals; the original signal and the reconstructed signal (*19*). This measure of similarity normalized to the original signal mean and used as a damage index is

$$DI_{RMSE} = \sqrt{\frac{\sum_{i=1}^{n} (x_i - y_i)^2}{\sum_{i=1}^{n} (x_i)^2}} \tag{9}$$

where x and y are the original or source signal and reconstructed signals respectively and n is the length or number of point in the signal.

4.2 Power Spectral Density (PSD)

PSD is a measure of the power in each frequency contained in a signal and is calculated using Welch‘s method. This method is used because it is said to have reduced noise in the power spectra estimate (*20*) and is calculated by dividing the signal into successive blocks and averaging the squared-magnitude of the discrete Fourier transform of the signal blocks. After calculating the PSD for a signal, the integral is taken to calculate the area under the PSD curve giving the average power of the signal over its bandwidth. A damage index based on the PSD and average power is formed by normalizing the difference in powers between the source and reconstructed signals and is given as

$$DI_{psd} = \frac{p_x - p_y}{p_x} \tag{10}$$

where x and y are the original or source signal and reconstructed signals respectively. Resulting values are between 0 (undamaged) and 1 (damaged).

4.3 Signal Maximum

A change in maximum value of the reconstructed signal is a direct indication that wave propagation is being disrupted along the propagation path. A damage index based on this measurement is formed by normalizing the difference in maximum values between the source and reconstructed signals and is given as

$$DI_{MAX} = \frac{(\,max(x) - max(y)\,)^2}{max(x)^2} \tag{11}$$

where x and y are the original or source signal and reconstructed signals respectively. Resulting values are between 0 (undamaged) and 1 (damaged).

4.4 Spectral Maximum

The spectral maximum is similar to the signal maximum in that changes in value indicate changes in the material or geometry along the propagation path. A damage index based on this measurement is formed by comparing the maximum amplitude spectra of the source and reconstructed signals and is give as

$$DI_{SPMX} = \frac{(\,max(X) - max(Y)\,)^2}{max(X)^2} \tag{12}$$

where X and Y are the source and reconstructed signals amplitude spectra respectively. Resulting values are between 0 (undamaged) and 1 (damaged).

5. Finite Difference Model and Simulations

A finite difference model was used to simulate wave propagation in a thin aluminum plate with notch. For this modeling and simulation commercial software (*21*) was used that is based on a finite difference algorithm (*22*) that solves a 2D (plane strain) acoustic wave equation. A schematic diagram of the finite difference time domain model is shown in figure 2. In this model, the ultrasonic source at position-A and receiver at position-B were each 10 mm in diameter and in planar contact with the sample surface positioned 100-mm apart. The aluminum plate had a thickness of 2.0 mm and width of 600 mm. A wide width was used to prevent interference of edge reflections. Aluminum properties of the material used in the model were; longitudinal velocity 6,420 m/s, transverse velocity 3,040 m/s, and density 2,700 kg/m^3.

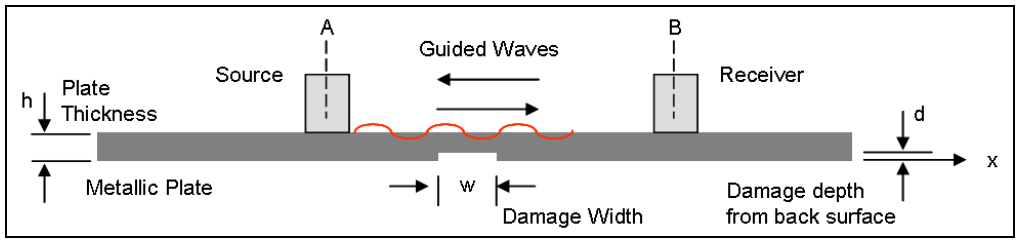

Figure 2. Finite difference model schematic.

The simulated damage (the notch) had a width of 6.0 mm and depth from the sample back surface that ranged from 0.0 to 1.0 mm in 0.1-mm steps. Notch depth translates to a depth to thickness ratio of 0% to 50%. To vary the location of the notch the source and receiver transducers could be repositioned, but always kept 100-mm apart. For example the notch was centered at 0.0 along the axis and the source was positioned at –40 mm and the receiver at 60 mm.

In simulations a broadband or narrowband source signal was used, both were available as functions in the modeling software. An example of the broadband pulse is shown in figure 3. Figure 3 (a) shows a Gaussian pulse with a center frequency of 0.5 MHz, duration of 5 µs, and bandwidth (FWHH) of 0.0 to 1.0 MHz. Figure 3 (b) show the spectrum of this signal. A narrowband pulse example is shown if figure 4. The waveform in figure 4 (a) shows the narrowband signal, a 5-cylce sine Gaussian pulse, with a center frequency of 0.5 MHz, duration of 13 µs, and bandwidth (FWHH) of 0.4 to 0.6 MHz.

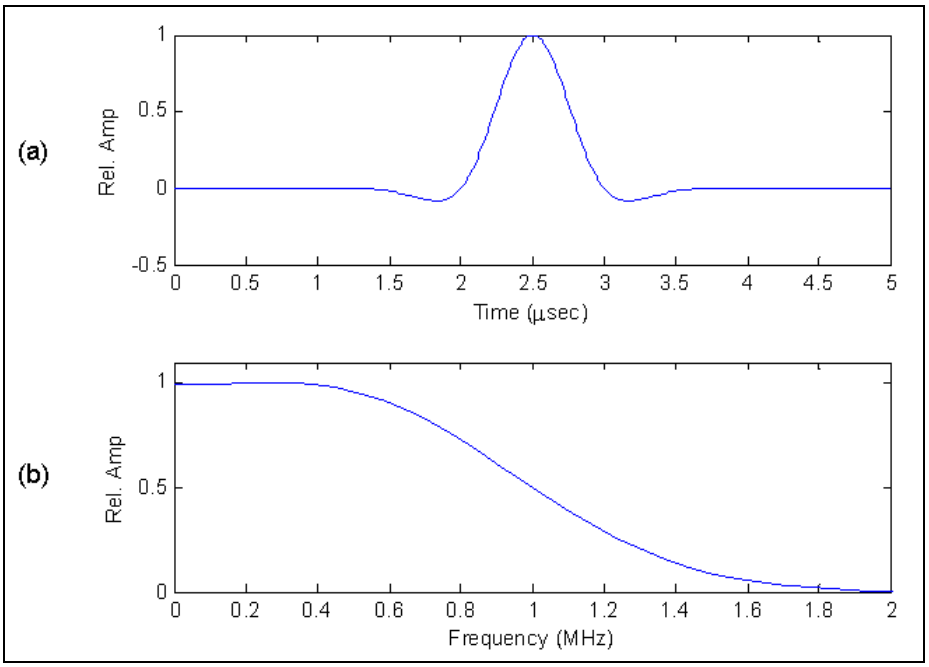

Figure 3. A broadband (a) signal and its (b) spectrum used in the simulation as a source function.

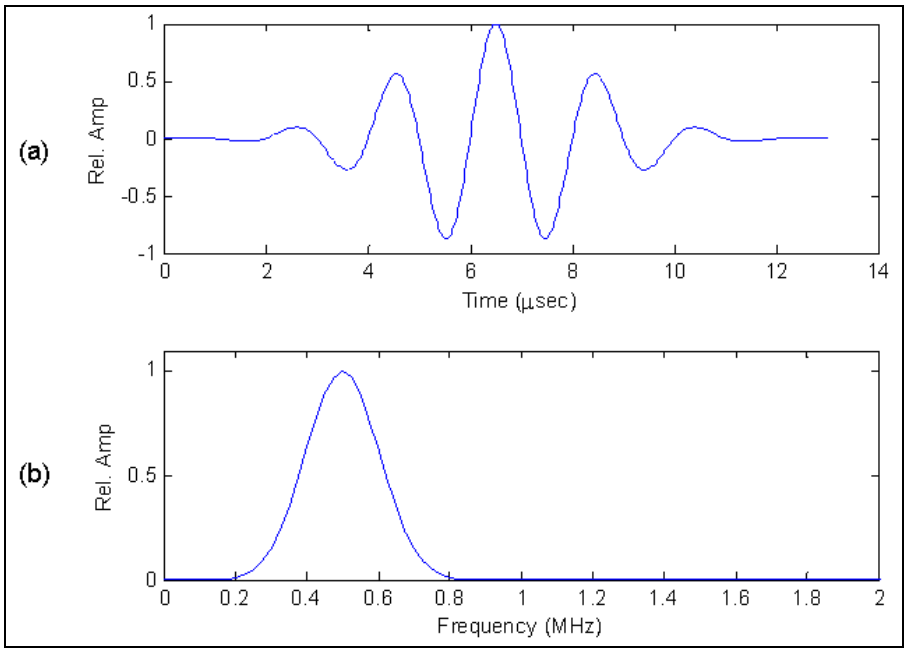

Figure 4. A narrowband (a) signal and its (b) spectrum used in the simulation as a source function.

Example temporal snapshots of guided waves propagation in the sample with a centrally located notch is shown in figure 5. This figure shows how the wave spreads as a function of time. An example receiver signal is shown in figure 6 where figure 6 (a) shows a signal for no damage and figure 6 (b) shows a signal for a centrally located notch with a 0.5-mm depth. For these signals the S_0 modes is located at ~20 µs and the A_0 mode starts at ~30 µs. The notches cause additional modes to propagate in the plate and are seen as perturbations in the guided wave signal shown in figure 6 (b) between the S_0 and A_0 modes.

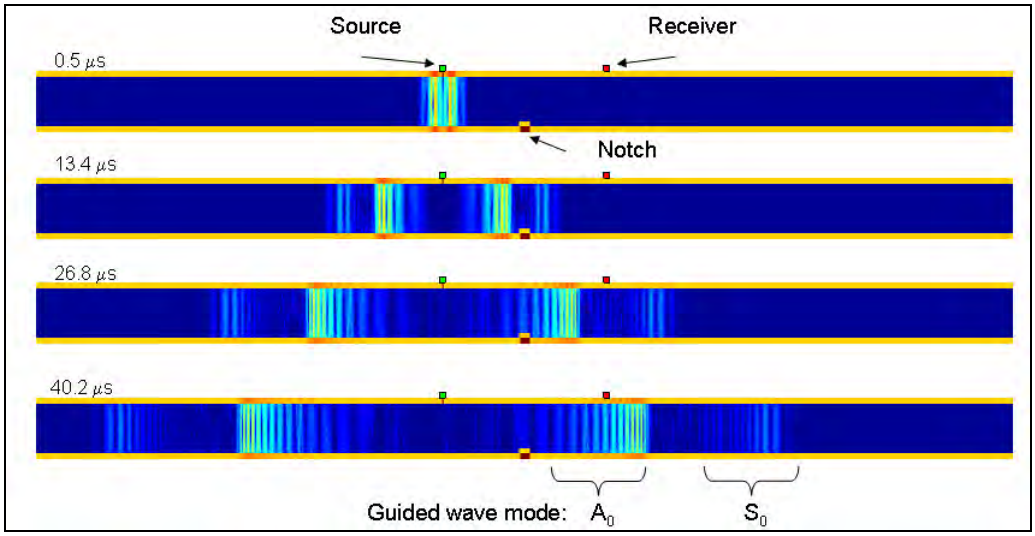

Figure 5. Typical snapshots of the guided wave propagating in the model.

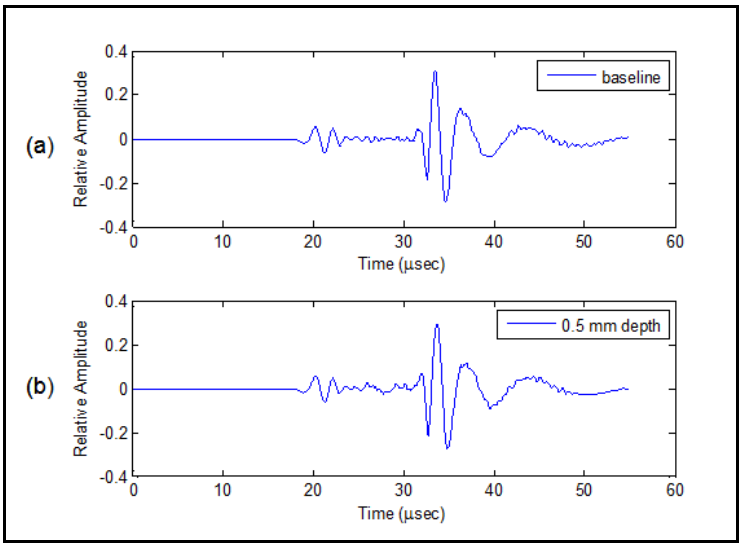

Figure 6. Simulated time-domain signal showing the primary symmetric and antisymmetric modes for (a) baseline signal without damage and (b) for a notch with 0.5-mm depth, source signal was a sine exponential pulse.

A time-frequency plot (or spectrogram) of the undamaged and damaged signals in figure 7 helps highlight the additional modes. A spectrogram of the undamaged signal is shown in figure 7 (a). In this spectrogram, the dispersion group velocity curves (the S_0, S_1, A_0, and A_1 modes) from figure 1 (b) are superimposed over the time-frequency map and illustrate the time-frequency and group velocity mapping for the given source bandwidth. Dispersion curve group velocity was converted to time using the source receiver separation distance as a conversion parameter. The intensity map shows the primary A_0 and S_0 Lamb wave modes and some higher modes with the S_0 mode arriving at about 18 µs and the A_0 mode arriving at about 30 µs. Frequency dispersion of the A_0 can be seen with the higher frequency modes arriving before the lower frequency modes. A spectrogram for the signal with damage is shown in figure 7 (b). This figure is similar to figure 7 (a) except for the region between the S_0 and A_0 modes at about 25 µs that shows a mode conversion resulting from the notch.

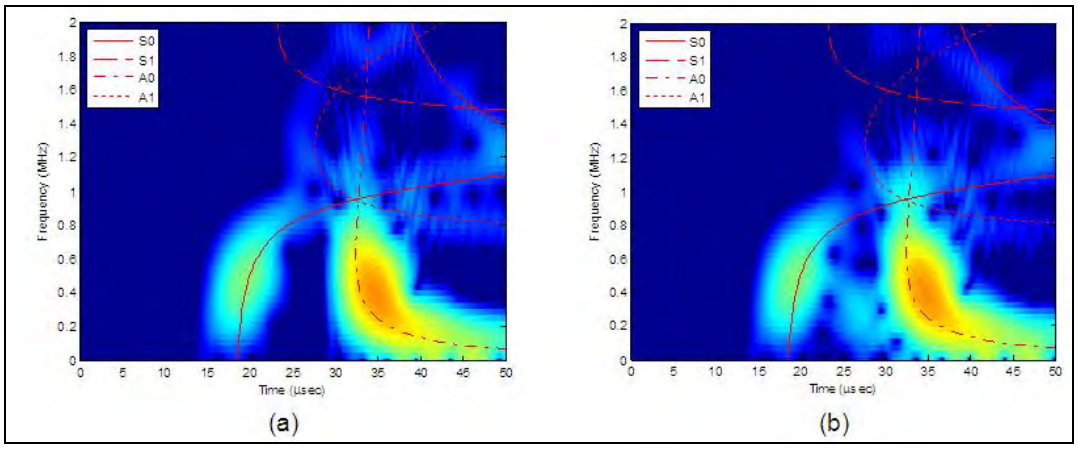

Figure 7. Spectrogram for (a) baseline signal and (b) signal with 0.5-mm depth notch for a sine exponential source signal.

For time-reversal simulations two separate models were used and were identical except for interchanging the source and receiver. The general time-reversal procedure as outline in section 3 was followed for narrowband and broadband sources and various notch depths. This procedure is illustrated in figure 8 for a broadband 0.5-MHz source, where figure 8 (a) shows the source signal transmitted at point-A, figure 8 (b) shows the received signal at point-B, and figure 8 (c) shows the time-reversed signal to be retransmitted at point-B. Similar signals for the narrowband 0.5-MHz source is shown in figure 9, where figure 9 (a) shows the source signal transmitted at point-A, figure 9 (b) shows the received signal at point-B, and figure 9 (c) shows the time-reversed signal to be retransmitted at point-B.

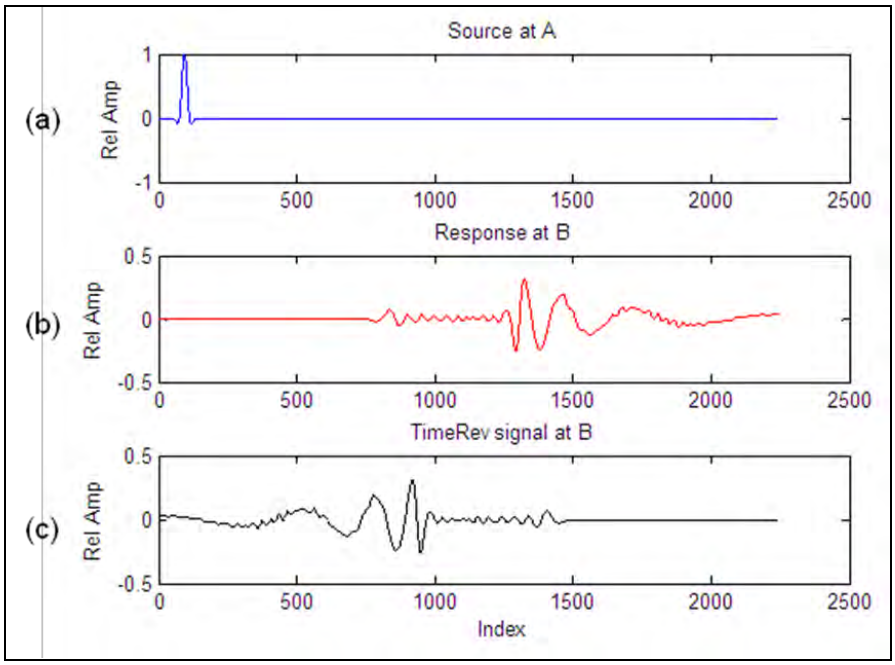

Figure 8. Illustration of the time reversal procedure (a) source signal broadband 0.5 MHz at point-A, (b) received signal at point-B, and (c) time-reversed signal at point-B.

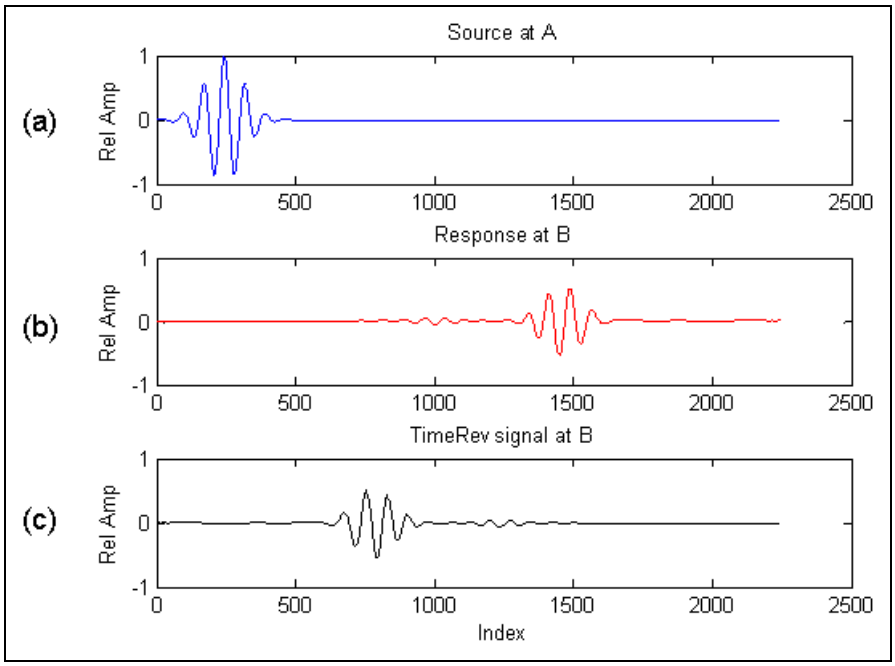

Figure 9. Illustration of the time reversal procedure (a) source signal narrowband at 0.50 MHz point-A, (b) received signal at point-B, and (c) time-reversed signal at point-B.

The resulting reconstructed signals for a narrowband and broadband source are shown in figure 10. In figure 10 (a) and (b) the source and reconstructed signals are superimposed and show that reconstructed signals are not exactly the same as the source signal, due to mode separation and dispersion, but in general confirms the time-reversal reconstruction process.

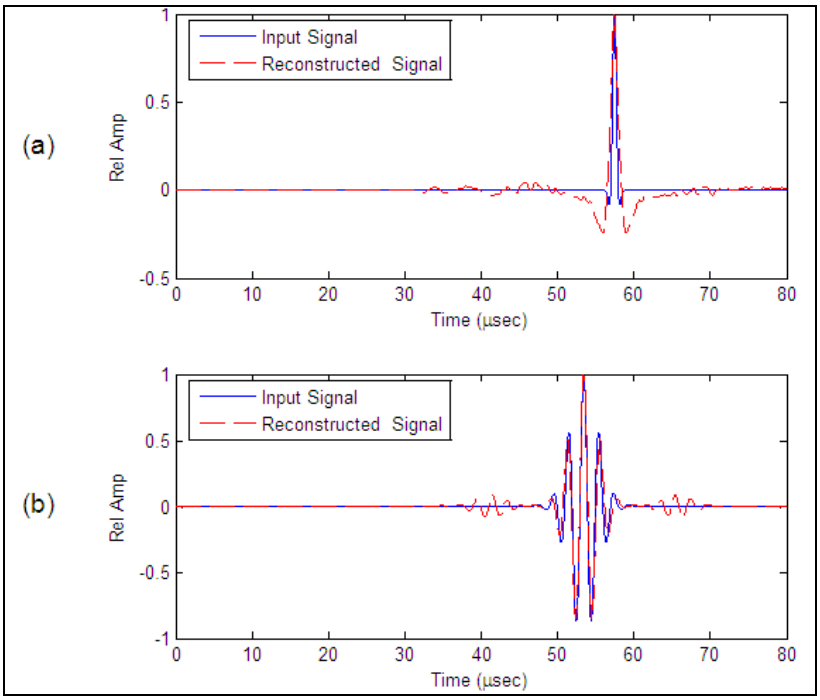

Figure 10. Normalized source and reconstructed signals for (a) broadband and (b) narrowband sources.

To help explain the side modes, the signal in figure 9 (c) was split into two separate signals as shown in figure 11. Figure 11 (a) shows the time reversed A_0 mode while figure 11 (b) shows the time reversed S_0 mode. Each of these signals was transmitted at point-B and received at point-A. The received signals are shown in figure 12. Figure 12 (a) shows the signal from A_0 mode source, figure 12 (b) shows the received signal from S_0 mode source, and figure 12 (c) shows the result of adding signals shown in figure 12 (a) and figure 12 (b). This result is directly comparable to the reconstructed signal in figure 10 (b) and illustrates that the side modes originate from mode conversion of the retransmitted A_0 and S_0 modes.

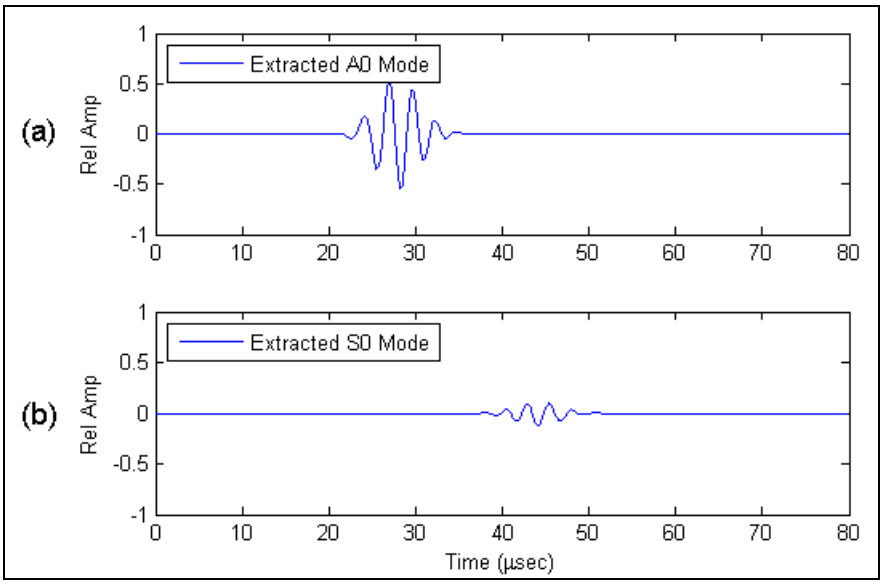

Figure 11. Extracted signals from figure 9c (a) extracted A_0 mode and (b) extracted S_0 mode.

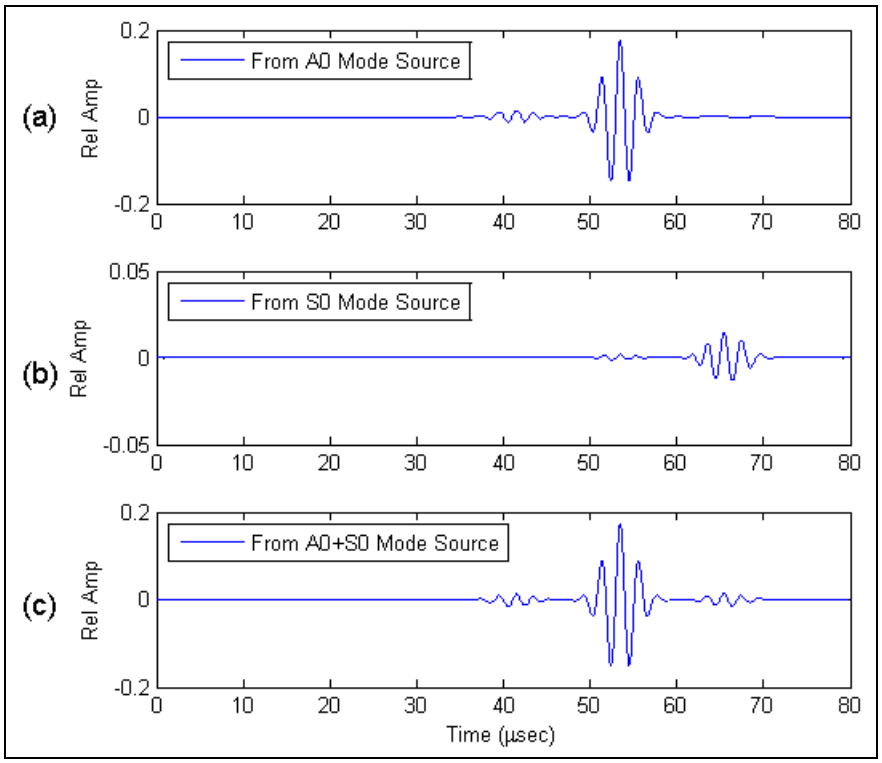

Figure 12. Received signals from extracted sources shown in figure 11 (a) received signal from A_0 mode source, (b) received signal from S_0 mode source, and (c) received signal shown in (a) and (b) added and directly comparable to the signal in figure 10 (b).

6. Results

A series of simulations were run for a broadband source with a center frequency of 0.5 MHz and narrowband sources with center frequencies of 0.25 MHz, 0.5 MHz, 0.75 MHz, and 1.0 MHz and notch depths of 0.0 mm to 1.0 mm in 0.2-mm increments. In each case, source and reconstructed signals were compared using damage index formulas described in section 4.

Resulting reconstructed signals for a broadband source at 0.50 MHz and a series of notch depth is shown in figure 13. Figure 13 (a) shows a larger amplitude main mode that is a reconstruction of the source signal through the TRM process and leading and trailing side modes that appear as low amplitude noise. To highlight the decreasing amplitude as a function of increasing notch depth an enlarged view of the main mode is shown in figure 13 (b). The amplitude spectrums of the signals in figure 13 (a) are shown in figure 13 (c) and show decreasing spectral amplitude as a function of increasing notch depth.

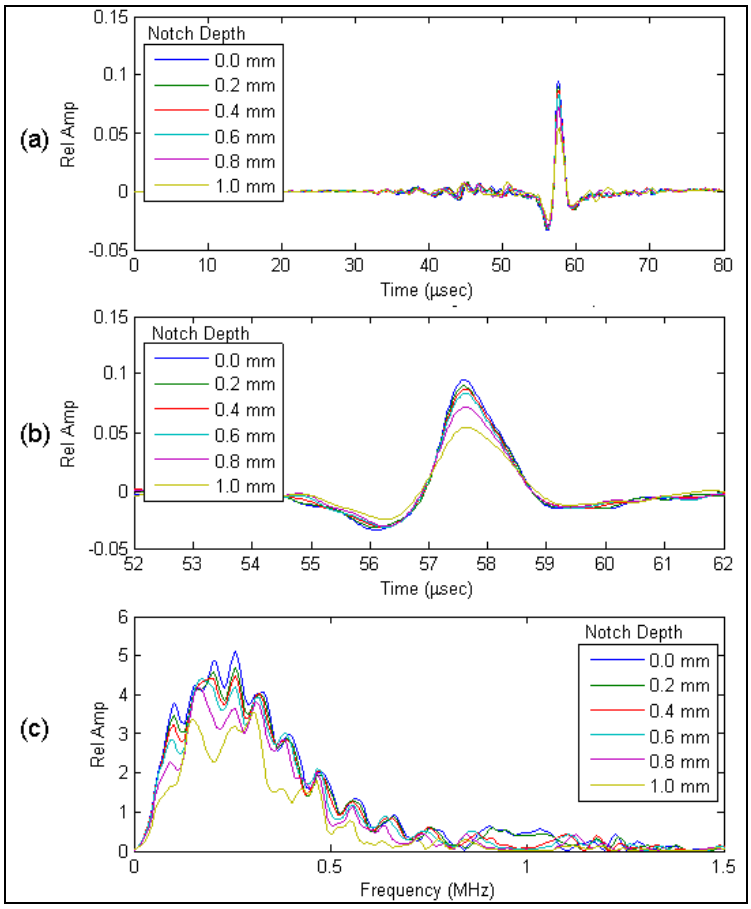

Figure 13. Reconstructed signals for a broadband source at 0.50 MHz (a) reconstructed signals, (b) enlarged views of main mode, and (c) amplitude spectrum.

Reconstructed signals for narrowband sources are shown in figure 14—figure (a) 0.25-MHz, (b) 0.50-MHz, (c) 0.75-MHz, and (d) 1.0-MHz center frequency. All the reconstructed signals show a larger main mode and lower amplitude leading and trailing side modes. In the 1.0-MHz case, the modes are not separated because of similar group velocity of the S_0 and A_0 and a higher order A_1 adding with the other modes. The amplitude spectrum for these signals is shown in figure 15—figure (a) 0.25-MHz, (b) 0.50-MHz, (c) 0.75-MHz, and (d) 1.0-MHz center frequency source signal and again the 1.0-MHz amplitude spectrums are not consistent due to mixing modes.

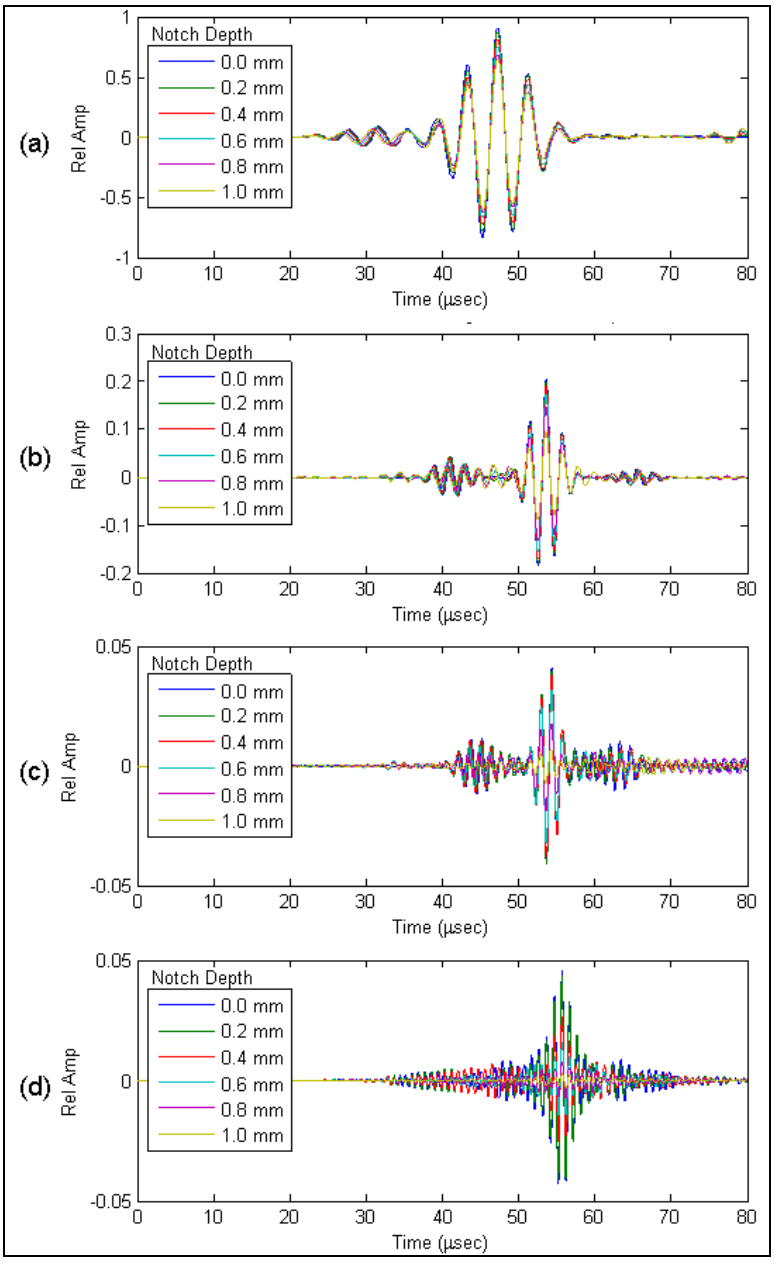

Figure 14. Reconstructed signals for narrowband sources (a) 0.25 MHz, (b) 0.50 MHz, (c) 0.75 MHz, and (d) 1.0 MHz.

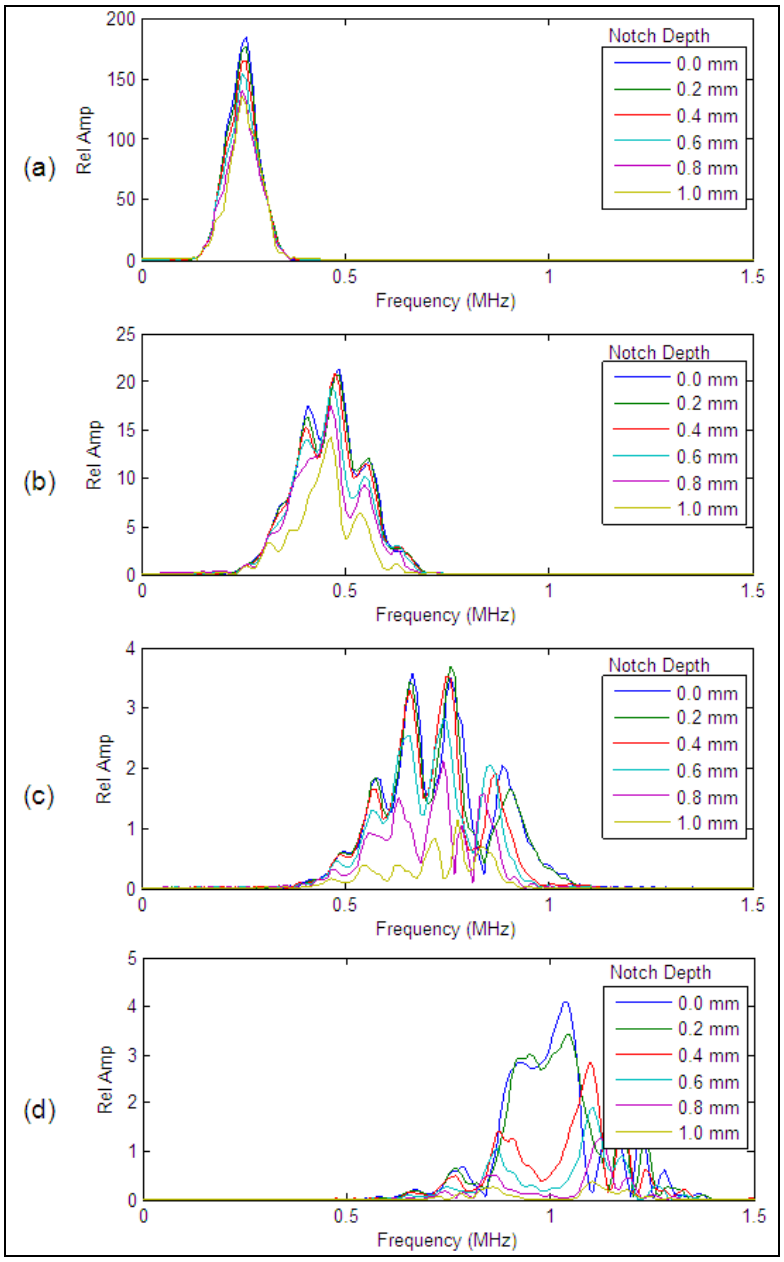

Figure 15. Amplitude spectrums for signals shown in figure 14; for source center frequencies of (a) 0.25 MHz, (b) 0.50 MHz, (c) 0.75 MHz, and (d) 1.0 MHz.

Calculated damage indexes for the broadband signals, as described in section 4, are shown in figure 16. The damage index values are shown to be increasing for increasing notch depth with an upward trend starting around a notch depth of 0.6 mm or damage depth of 30% of material thickness. Damage index values for the narrow band signals are shown in figures 17, 18, 19, and 20 for center frequencies of 0.25 MHz, 0.50 MHz, 0.75 MHz, and 1.0 MHz, respectively. Again, the damage index values are increasing for increasing notch depth with an upward trend starting around a notch depth of 0.4 mm or damage depth of 20% of material thickness. The damage

index values for the 1.0-MHz case is inconsistent with the other center frequency cases: most likely due to mixing of higher and lower order modes.

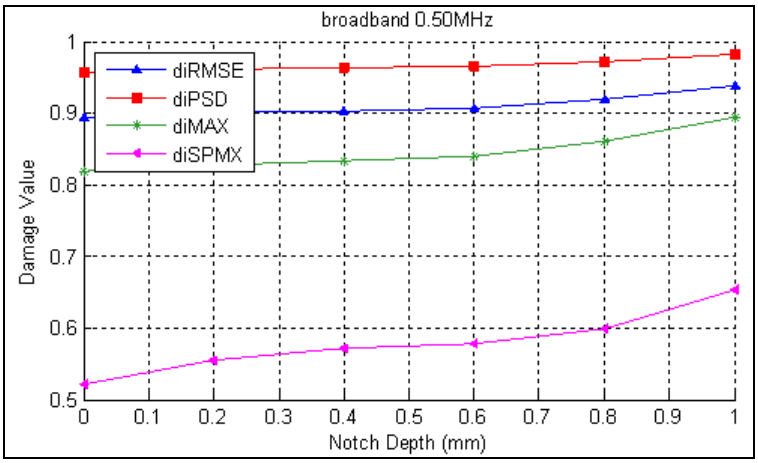

Figure 16. Damage index values, as described in section 4, for broadband signals as a function of notch depth.

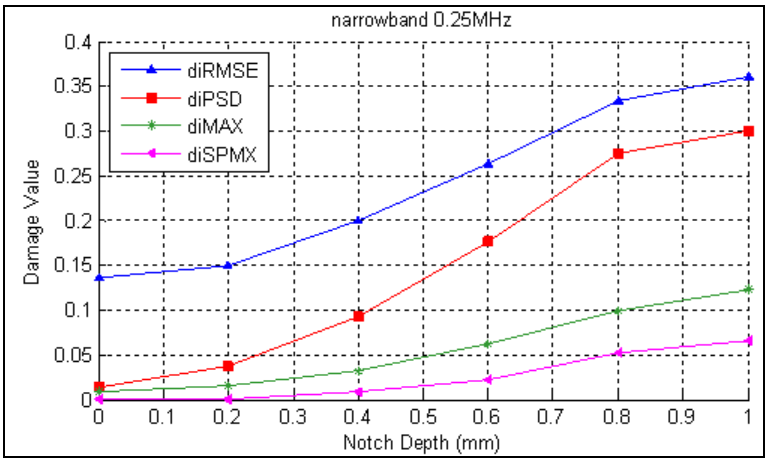

Figure 17. Damage index values, as described in section 4, for narrowband signals at a center frequency of 0.25 MHz as a function of notch depth.

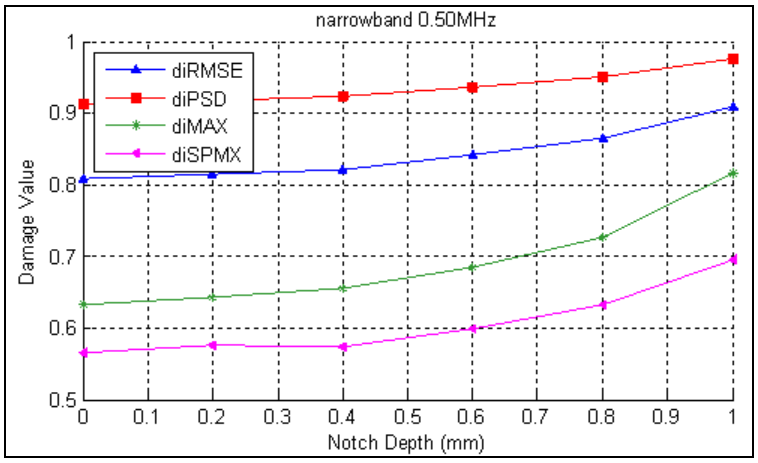

Figure 18. Damage index values, as described in section 4, for narrowband signals at a center frequency of 0.50 MHz as a function of notch depth.

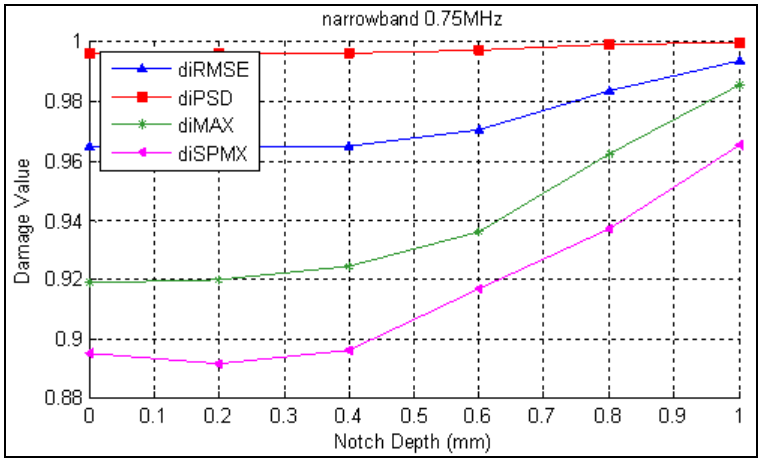

Figure 19. Damage index values, as described in section 4, for narrowband signals at a center frequency of 0.75 MHz as a function of notch depth.

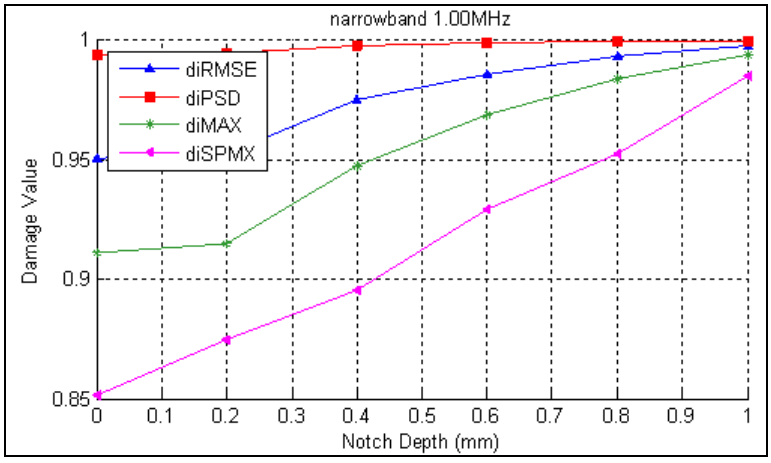

Figure 20. Damage index values, as described in section 4, for narrowband signals at a center frequency of 1.00 MHz as a function of notch depth.

7. Conclusions

Time reversal methods for ultrasonic guided waves were examined as a means of detecting damage in metallic plate structures. This examination was performed using a finite difference model of a metallic plate with a central notch of various depths, to simulate damage and generate signals for analysis. According to this method the input signal to a system can be reconstructed if a response signal obtained from another point is emitted back to the original point after being reversed in time. This argument was originally put forth and proven for bulk wave propagation and was shown to hold up for dispersive lamb wave propagation. With this method, damage diagnosis lies in the premise that the time reversibility breaks down when a defect such as damage exists along the wave propagation path. The defect can then be sensed by correlating the reconstructed signal with the original signal. This was explored by transmitting broadband and narrowband source signals and comparing them with their corresponding reconstructed signal in the form of a damage index.

Results showed that narrowband excitation is somewhat more sensitive than broadband excitation to notch depth. The broadband excitation could detect a notch to a depth of 0.6 mm or 30% material thickness loss and the narrowband excitation could detect a notch to a depth of 0.4 mm or 20% material thickness. It is theorized that the narrowband is more sensitive due to better single mode isolation.

Although the time reversal method requires some manipulation of time recorded signals the process is relatively straight forward and eliminates the need to record a separate baseline for every potential source and receiver. Thus time reversal technique for analysis of ultrasonic lamb waves is a viable method for monitoring of damage in materials of plate geometry.

8. References

1. Rose, J. L. Ultrasonic Guided Waves in Structural Health Monitoring. *Key Engineering Materials* **2004**, *270–273*, 14–21.
2. Rose, J. L. Recent Advances in Guided Wave NDE. *IEEE Ultrasonics Symposium,* pp. 761–770, 1995.
3. Fink, M. Time Reversal of Ultrasonic Fields-Part I: Basic Principles. *IEEE Transactions on Ultrasonics, Ferroelectronics, and Frequency Control* **1992**, *39* (5), 555–566.
4. Wu, F.; Thomas, J.; Fink, M. Time Reversal of Ultrasonic Fields-Part II: Experimental Results. *IEEE Transactions on Ultrasonics, Ferroelectronics, and Frequency Control* **1992**, *39* (5), 567–578.
5. Fink, M. Time-Reversed Acoustic. *Scientific American* **1999**, *281*, 91–97.
6. Chakroun, N.; Fink, M.; Wu, F. Ultrasonic Nondestructive Testing with Time Reversal Mirrors, Proc. *IEEE Ultrasonic Symposium*, Tucson, 2, 809–814, 1992.
7. Chakroun, N.; Fink, M.; Wu, F. Time Reversal Processing in Ultrasonic Nondestructive Testing. *IEEE Transactions on Ultrasonics, Ferroelectrics and Frequency Control* **1995**, *42*, 1087–1098.
8. Roux, P.; Roman, B.; Fink, M. Time-Reversal in an Ultrasonic Waveguide. *Applied Physics Letters* **1997**, *70* (14), 1811–1813.
9. Ing, R. K.; Fink, M. Time-Reversed Lamb Waves. *IEEE Transactions on Ultrasonics, Ferroelectrics and Frequency Control* **1998**, *45*, 1032–1043.
10. Prada, C.; Kerbrat, E.; Cassereau, D.; Fink, M. Time Reversal Techniques in Ultrasonic Nondestructive Testing of Scattering Media. *Inverse Problems* **2002**, *18*, 1761–1773.
11. Wang, C. H.; Rose, J. L.; Chang, F. A Computerized Time-Reversal Method for Structural Health Monitoring, NDE and Health Monitoring of Aerospace Materials and Composites II. Andrew L. Gykenyesi, Peter J. Shull, Editors, *Proceedings of SPIE,* Vol. 5046, pp 48–58, 2003.
12. Wang, C. H.; Rose, J. L.; Chang, F. A Synthetic Time-Reversal Imaging Method for Structural Health Monitoring. *Smart Materials and Structures* **2004**, *13*, 415–423.
13. Xu, B.; Giurgiutiu, V. Single Mode Tuning Effects on Lamb Wave Time Reversal with Piezoelectric Wafer Active Sensors for Structural Health Monitoring. *J Nondestruct Eval* **2007**, *26*, 123–134.

14. Auld, B. A. *Acoustic Fields and Waves in Solids, Volume II*; Robert E. Krieger Publishing Company, 1990.

15. Achenbach, J. D. *Wave Propagation in Elastic Solids*; Elsevier Science Publishers, 1999.

16. Viktrorov, I. A. *Rayleigh and Lamb Waves*; Plenum Press, 1967.

17. Rose, J. L. *Ultrasonic Waves in Solid Media*; Cambridge University Press, 1999.

18. Pavlakovic, B.; Lowe, M.J.S. *Disperse*, An interactive program for generating dispersion curves, Imperial College NDT Lab., London, UK, 2001.

19. Root mean square deviation. (2011, February 25). In *Wikipedia, The Free Encyclopedia*. Retrieved 12:48, April 22, 2011, from http://en.wikipedia.org/w/index.php?title=Root_mean_square_deviation&oldid=415919654

20. Welch's method. (2010, May 14). In *Wikipedia, The Free Encyclopedia*. Retrieved 15:29, April 21, 2011, from http://en.wikipedia.org/w/index.php?title=Welch%27s_method&oldid=362073495

21. Cyberlogic, Inc., *Wave2000, v1.00a,* A stand-alone computer software program for computational ultrasonics, New York, NY, 1997.

22. Schechter, R. S.; Chaskelis, H. H.; Mignogna, R. B.; Delsanto, P. P. Real-time Parallel Computation and Visualization of Ultrasonic Pulses in Solids. *Science* **1994**, *265*, 1188–92.

List of Symbols, Abbreviations, and Acronyms

A_0	antisymmetric mode
c_L	longitudinal velocity
c_T	transverse velocity
DI	damage index
MAX	maximum value
PSD	power spectral density
RMSE	root mean square error
S_0	symmetric mode
SPMX	signals amplitude spectrum
TRM	time-reversal methods
ρ	density

NO. OF COPIES	ORGANIZATION
1 (PDF only)	DEFENSE TECHNICAL INFORMATION CTR DTIC OCA 8725 JOHN J KINGMAN RD STE 0944 FORT BELVOIR VA 22060-6218
1	DIRECTOR US ARMY RESEARCH LAB IMNE ALC HRR 2800 POWDER MILL RD ADELPHI MD 20783-1197
1	DIRECTOR US ARMY RESEARCH LAB RDRL CIO LL 2800 POWDER MILL RD ADELPHI MD 20783-1197
1	DIRECTOR US ARMY RESEARCH LAB RDRL CIO MT 2800 POWDER MILL RD ADELPHI MD 20783-1197
5 HC 1 CD	R F ANASTASI 14 HOLLOWAY DRIVE HAMPTON VA 23666

INTENTIONALLY LEFT BLANK.